Nonlinear Control for Magnetic Levitation of Automotive Engine Vales

K. S. Peterson, *Member, IEEE*, J. W. Grizzle, *Fellow, IEEE*, and A. G. Stefanopoulou, *Member, IEEE*

***Abstract*—Position regulation of a magnetic levitation device is achieved through a control Lyapunov function (CLF) feedback design. It is shown experimentally that by selecting the CLF based on the solution to an algebraic Riccati equation it is possible to tune the performance of the controller using intuition from classical LQR control. The CLF is used with Sontag's universal stabilizing feedback to provide enhanced transient performance farther away from the origin than was achieved with the LQR controller.**

***Index Terms*—Actuators, electromagnets, engines, nonlinear systems, optimal control.**

I. Introduction

ELECTROMAGNETIC levitation is a classic control problem for which numerous solutions have been proposed. Many of the proposed solutions have focused on the use of feedback linearization [3], [9]–[11], [16] due to the nonlinear characteristics of the magnetic and electric subsystems. Unfortunately, feedback linearization requires a very accurate model which may be unrealistic near the electromagnet due to magnetic saturation and eddy current effects, thereby limiting the range of motion achievable in the closed-loop system. Sliding mode [1], [2], [13] and H_∞ [15], [21] control have been used to account for the changing local dynamics and to provide robustness against unmodeled nonlinearities present in the system. Linearization and switching can be avoided through the application of nonlinear control based on backstepping [5], [6] and passivity [19].

The control design investigated here is based on control Lyapunov functions (CLFs) and Sontag's universal stabilizing feedback [17]. The control Lyapunov function is selected based on a solution to an algebraic Riccati equation to allow us to "tune" the controller for performance. Neither current control nor a static relationship between current, voltage, and the magnetic force is assumed, as done by Velasco-Villa [19] and Green [6]. Instead, the dynamics of the current/flux are compensated through the use of a full-state feedback/observer structure. Implementation is achieved using position and current sensors, a nonlinear observer to estimate velocity, a novel method to estimate the magnetic flux, and voltage control. To demonstrate the effectiveness of the controller, it is experimentally evaluated on an electromagnetic valve actuator (EVA)designed for use in the actuation of automotive engine valves.

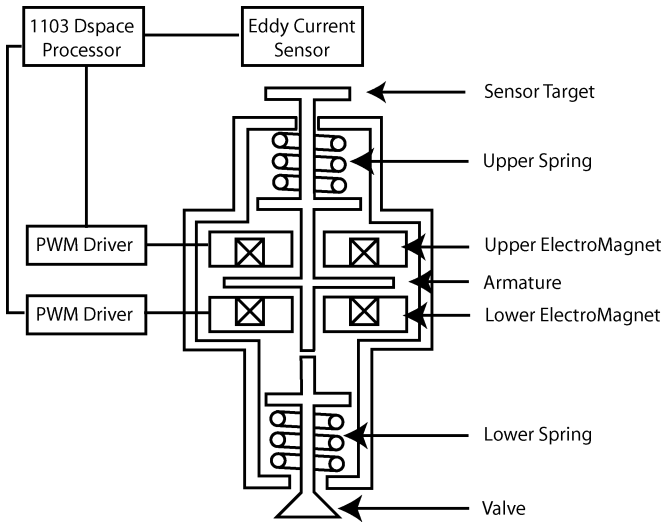

Fig. 1. Electromagnetic valve actuator and experimental setup.

II. Electromagnetic Valve Actuator (EVA)

The EVA, shown in Fig. 1, has recently received attention due to its potential to improve the performance of the standard internal combustion engine. Valve motion in most automotive engines is controlled via a camshaft, which mechanically links the valve motion to the motion of the crankshaft. By decoupling the valve motion from the crankshaft, the EVA allows for more flexibility in optimizing fuel economy, torque, and emissions [8]. In addition to providing variable valve timing, the EVA is capable of achieving variable valve lift through magnetic levitation. With the exception of our previous work [12], research on the control of the EVA has primarily focused on the elimination of large impacts that occur between the armature and lower and upper magnetic coils. In this paper we expand on our previous work [12], which only briefly touched on the subject of magnetic levitation.

The EVA governs the valve motion in the following manner. The armature is initially held against the upper magnetic coil, causing the valve to seal off the engine cylinder. In this position, the upper spring is more compressed than the lower spring creating a force imbalance as the upper and lower springs are identical. When the valve open command is issued, the current in the upper magnetic coil is reduced to zero and the potential energy stored in the upper spring drives the armature downward, causing the valve to open. Depending on the command to the actuator, two outcomes are possible. In the case of full valve opening, the lower magnetic coil is used to bring the armature

Manuscript received October 4, 2004; revised March 9, 2005. Manuscript received in final form November 15, 2005. Recommended by Associate Editor B. de Jager. This work was supported in part by the National Science Foundation (NSF) and the Ford Motor Company.

K. S. Peterson is with the School of Mechanical Engineering, Purdue University, West Lafayette, IN 47907 USA (e-mail: petersonks@ecn.purdue.edu).

J. W. Grizzle is with the Electrical Engineering and Computer Science Department, University of Michigan, Ann Arbor, MI 48109 USA (e-mail: grizzle@eecs.umich.edu).

A. G. Stefanopoulou is with the Department of Mechanical Engineering and Applied Mechanics, University of Michigan, Ann Arbor, MI 48109 USA (e-mail: annastef@umich.edu).

Digital Object Identifier 10.1109/TCST.2005.863669

in contact with the lower electromagnet, and held there. From the view point of stability, this is the trivial case as the armature can be held against the lower magnetic coil by applying a sufficiently large constant voltage command. In the case of partial valve lift, the electromagnets are used to hover the armature. As the electromagnets can only apply attractive forces, the upper magnetic coil is used to hover the armature above the mid-position and the lower magnetic coil is used to hover the armature below the mid-position. When the valve closed command is issued, the upper magnetic coil and any potential energy stored in the lower spring are used to return the armature/valve to the closed position.

Hovering the armature is slightly different than the classic control problem of magnetic levitation due to the presence of the springs. When both electromagnets are deenergized, the armature sits at rest equidistant from the electromagnets. As shown by Tai [18], any equilibrium position that is greater than 1/3 the full lift away from either electromagnet is open-loop exponentially stable. However, the presence of the springs does not necessarily make the control problem appreciably easier. As the springs are extremely stiff, the bandwidth of the mechanical subsystem is on the order of the bandwidth of the electrical subsystem. Therefore, it is not practical to assume current control. In addition, the regions of attraction of the open-loop stable equilibria are small. It was found experimentally that the armature had to start at rest equidistant from the electromagnets in order to achieve stable open-loop hovering for equilibrium positions greater than 1/3 the full lift away from either electromagnet. If the armature starts at rest against the upper magnetic coil, application of the open-loop equilibrium voltage results in the armature being brought into contact with the activated electromagnet. As the latter initial condition is the one experienced during operation, it is necessary to design a closed-loop controller to enlarge the region of attraction so that hovering is achieved for both open-loop stable and unstable equilibrium positions.

III. Modeling the EVA

As derived by Wang [20], the dynamics of the EVA are given by[1]

$$\begin{aligned}\frac{dz}{dt} &= v\\ \frac{dv}{dt} &= \frac{1}{m}\left(F^u_{\text{mag}} - F^l_{\text{mag}} + k_s(l-z) - bv\right)\\ \frac{d\lambda_l}{dt} &= V_l - \frac{r\lambda_l(k_b+z)}{k_a}\\ \frac{d\lambda_u}{dt} &= V_u - \frac{r\lambda_u(k_b+2l-z)}{k_a}\end{aligned}$$

where z (m) is the distance between the armature and the lower coil, v (m/s) is the velocity of the armature, λ_l (Vs) is the magnetic flux in the lower coil, λ_u (Vs) is the magnetic flux in the upper coil, m (kg) is the combined mass of the armature and valve, F^l_{mag} (N) is the magnetic force generated by the lower coil, F^u_{mag} (N) is the magnetic force generated by the upper coil,

[1]The original model is derived in terms of current rather than flux. However, the flux based representation is mathematically simpler.

TABLE I
Numerical Values of Constants

Parameter	Numerical value	Parameter	Numerical value
m	0.27 kg	k_b	$4.0 \cdot 10^{-5}$ m
k_s	$158 \cdot 10^3$ N/m	l	$4.0 \cdot 10^{-3}$ m
b	7.53 kg/s	r	6.0 Ω
k_a	$29.92 \cdot 10^{-6}$ Nm^2/A^2		

k_s (N/m) is the spring constant, l (m) is half the total armature travel, b (kg/s) is the damping coefficient, V_l (V) is the voltage applied to the lower coil, V_u (V) is the voltage applied to the upper coil, and r (Ω) is the combined resistance of the wiring and magnetic coil. The constants k_a and k_b are fit based on experimental data as described in [20]. Numerical values for all constants are found in Table I. Finally, the magnetic force generated by either coil is given by

$$F_{\text{mag}} = \frac{\lambda^2}{2k_a}. \tag{1}$$

This model assumes that the effects of eddy currents, magnetic saturation, and static friction are negligible. It is important to note however that the functional form of the magnetic force given in (1) is independent of magnetic saturation. This is an important property that will be exploited later when an observer is designed.

As explained in Section II, only one electromagnet is used to hover the armature. Therefore, without loss of generality we assume the lower coil is used and neglect the dynamics of the upper coil. To simplify the controller design, a new input u and coordinates $x = [x_1\ x_2\ x_3]$ are introduced per

$$\begin{aligned}x_1 &= z - z_{\text{eq}}\\ x_2 &= v\\ x_3 &= \lambda_l - \lambda_{\text{eq}}\\ u &= V_l - V_{\text{eq}},\end{aligned}$$

where z_{eq}, λ_{eq}, and V_{eq} are the equilibrium position, flux, and voltage, respectively. The equilibrium point is now located at the origin, and the system dynamics are represented in the form

$$\frac{dx}{dt} = f(x) + g(x)u \tag{2}$$

where

$$f(x) = \begin{bmatrix} x_2 \\ \frac{1}{m}\left(-\frac{x_3^2}{2k_a} - k_s x_1 - bx_2 - \frac{x_3\lambda_{\text{eq}}}{k_a}\right) \\ -\frac{x_3(k_b+z_{\text{eq}}+x_1)r}{k_a} + \frac{x_1\lambda_{\text{eq}}r}{k_a}\end{bmatrix}$$

$$g(x) = [0 \quad 0 \quad 1]^T.$$

A frequent assumption in the control of electromagnetic actuators is that the dynamics of the current/flux are significantly faster than the dynamics of the mechanical components of the system. This assumption reduces the complexity of the control problem as most of the nonlinearities are present in the dynamics of current/flux. Unfortunately, this assumption is not valid for our system. The bandwidth of position is approximately equal to the bandwidth of current/flux due to the presence of stiff springs.

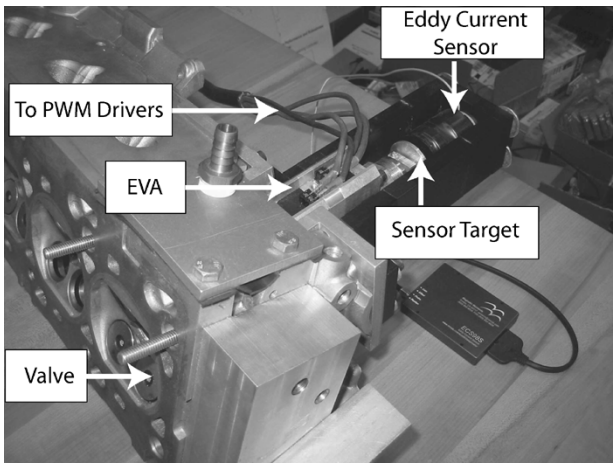

Fig. 2. Experimental setup.

IV. Experimental Setup

The experimental results which follow are conducted on the setup shown schematically in Fig. 1 and pictorially in Fig. 2, consisting of:

- a prototype 200 V electromechanical valve actuator;
- a 200 V power supply (Power-Ten Inc. Model Number:P83) (not shown);
- two pulsewidth modulated (PWM) brush type servo amplifiers (Advanced Motion Controls, Model Number:50A-DD);
- a dSpace 1103 processing board;
- an eddy current sensor (Magnetic Moments:ECS985).

The position of the armature is determined from the eddy current sensor that detects changes in a self-generated magnetic field caused by the motion of the sensor target. The current in each coil is measured by built-in sensors in the PWM drivers. The analog signals from the PWM drivers and the eddy-current sensors are sampled by the dSpace 1103 processor at 20 kHz in order to determine the duty cycle applied to each PWM driver based on the control algorithm. We assume that the PWM drivers are sufficiently fast that the applied voltage is equivalent to the commanded duty cycle multiplied by the supply voltage of 180 V.

In the results that follow in Figs. 3–6, 11, 13, and 14, the upper magnetic coil is located at $z = 8$ mm, the lower magnetic coil is located at $z = 0$ mm, the signal shown is the unfiltered position based on the eddy current sensor mounted on the rear of the actuator, and the armature is released from rest against the upper magnetic coil at the beginning of the experiment.

V. Controller Design

The proposed controller consists of two components, a stabilizing controller to achieve hovering and a damping controller that retards the initial motion of the armature during release. The stabilizing controller is based on Sontag's universal stabilizing

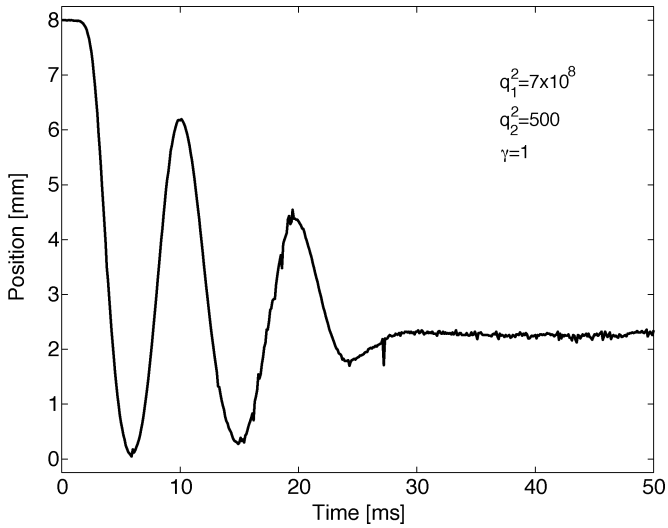

Fig. 3. Stable hovering achieved with the CLF given in (6) on the experimental setup described in Section IV.

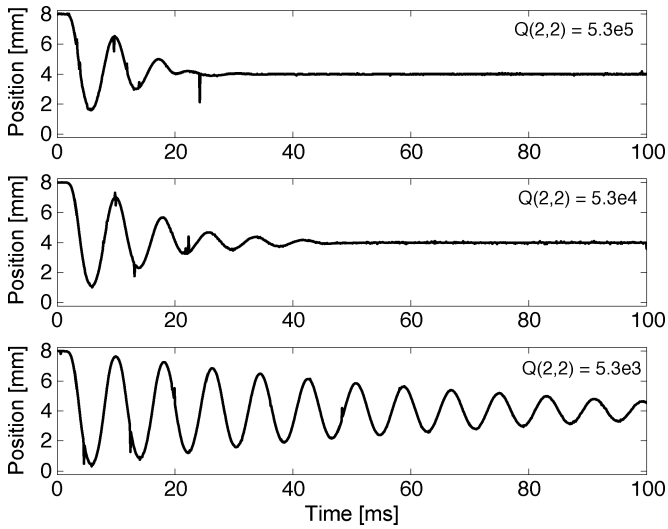

Fig. 4. Effects of tuning the matrix Q determined experimentally on the setup described in Section IV.

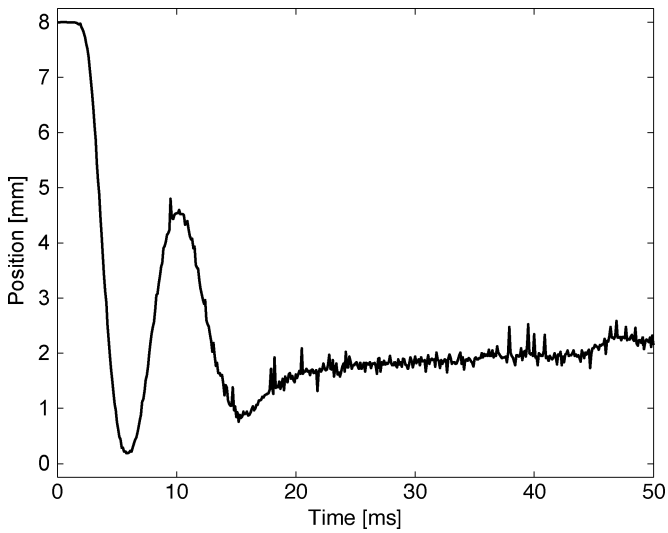

Fig. 5. Stable hovering achieved with the LQ-CLF on the experimental setup described in Section IV.

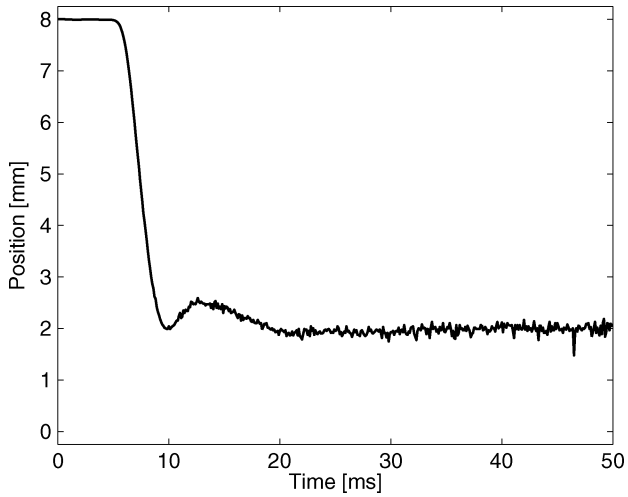

Fig. 6. Stable hovering achieved with the LQ-CLF and dampened release on the experimental setup described in Section IV.

feedback [17]. Two different CLFs for use with Sontag's feedback are given. The resulting performance achieved by the first CLF is quite poor, motivating the selection of a new CLF based on the solution to an algebraic Riccati equation. Experimental results are given to show that selecting the CLF in this manner enables the designer to tune for performance. Since the electromagnet can only apply attractive forces, the upper coil is used to slow the release of the armature to reduce overshoot near the lower coil.

A. Stabilizing Controller

As the flux dynamics are nonnegligible, see Section III, we have used Sontag's feedback [17] to stabilize the three state system. Given a candidate Lyapunov function V such that

$$V(x) \geq 0 \; \forall x \in R^3 \tag{3}$$
$$V(x) = 0 \text{ iff } x = 0 \tag{4}$$

it is said to be a CLF if there exists $\delta > 0$ s.t.

$$L_g V(x) = 0 \Rightarrow L_f V(x) < 0 \tag{5}$$

for all $x \neq 0$ such that $\|x\| < \delta$, where $L_f V$ and $L_g V$ are the Lie derivatives of the CLF, defined as

$$L_f V(x) = \frac{\partial V}{\partial x} f(x) \quad \text{and} \quad L_g V(x) = \frac{\partial V}{\partial x} g(x).$$

If the conditions given in (3)–(5) are satisfied, then Sontag's feedback given as

$$u = \begin{cases} -\frac{L_f V + \sqrt{L_f V^2 + ((L_g V)(L_g V)^T)^2}}{L_g V}, & \text{for } L_g V \neq 0 \\ 0, & \text{for } L_g V = 0 \end{cases}$$

renders the origin asymptotically stable.

To implement Sontag's feedback, we propose the function

$$V(x) = [x_1 \quad x_2] P_{nl} [x_1 \quad x_2]^T + \gamma x_3^2 \tag{6}$$

as a candidate CLF, where γ is constant and positive and the matrix P_{nl} satisfies the Lyapunov equation

$$A_{nl}^T P_{nl} + P_{nl} A_{nl} + Q_{nl} = 0$$

where

$$A_{nl} = \begin{bmatrix} 0 & 1 \\ -\frac{k_s}{m} & -\frac{b}{m} \end{bmatrix}$$
$$Q_{nl} = \begin{bmatrix} q_1^2 & 0 \\ 0 & q_2^2 \end{bmatrix}.$$

Since A_{nl} is Hurwitz and Q_{nl} is positive definite, the matrix P_{nl} is positive definite. Solving for $L_g V$ yields

$$\begin{aligned} L_g V(x) &= \begin{bmatrix} \frac{dV}{dx_1} & \frac{dV}{dx_2} & \frac{dV}{dx_3} \end{bmatrix} [0 \quad 0 \quad 1]^T \\ &= 2\gamma x_3. \end{aligned}$$

Therefore

$$L_g V(x) = 0 \text{ iff } x_3 = 0. \tag{7}$$

When $x_3 = 0$, $L_f V$ is given as

$$\begin{aligned} L_f V(x) &= \left(\begin{bmatrix} \frac{dx_1}{dt} & \frac{dx_2}{dt} \end{bmatrix} P_{nl} [x_1 \quad x_2]^T \right. \\ &\qquad \left. + [x_1 \quad x_2] P_{nl} \begin{bmatrix} \frac{dx_1}{dt} & \frac{dx_2}{dt} \end{bmatrix}^T \right) \\ &= \left([x_1 \quad x_2] A_{nl}^T P_{nl} [x_1 \quad x_2]^T \right. \\ &\qquad \left. + [x_1 \quad x_2] P_{nl} A_{nl} [x_1 \quad x_2]^T \right) \\ &= - [x_1 \quad x_2] Q_{nl} [x_1 \quad x_2]^T \end{aligned}$$

showing that (6) is a Control Lyapunov function.

Formulating Sontag's feedback based on (6) and implementing it on the experimental setup described in Section IV, we are able to achieve stable hovering as shown in Fig. 3. However, the performance is quite oscillatory. By adjusting q_1, q_2, and γ, it is possible to affect the performance, but it is not obvious how they should be manipulated to achieve the desired results. For this reason, a better candidate CLF is sought.

Let us instead select the CLF[2] to be

$$V(x) = x^T P x \tag{8}$$

where the matrix P satisfies the algebraic Riccati equation

$$PA + A^T P + Q - PBB^T P = 0$$

for

$$A = \left. \frac{\partial f(x)}{\partial x} \right|_{x=0} \tag{9}$$
$$B = g(x) \tag{10}$$
$$Q > 0. \tag{11}$$

For convenience, the CLF given in (8) will henceforth be referred to as the LQ-CLF. The motivation in selecting the CLF in

[2]The Lyapunov function $V = x^T P x$ is a global CLF for the linearized system by Khalil [7], Exercise 3.25. Thus, by Lyapunov's indirect method, Thm. 3.7 [7], V is a (local) CLF for the nonlinear system.

this manner is that we hope to influence the performance of the system by manipulating the LQR cost function

$$J = \int_0^\infty (x^T Q x + u^2) dt \tag{12}$$

subject to the dynamics

$$\frac{dx}{dt} = Ax + Bu \tag{13}$$

in order to select P. Note that even though we have chosen a quadratic Lyapunov function based on the linearized system model, the full nonlinear model is used when formulating Sontag's feedback.

Sepulchre [14] has shown that Sontag's feedback is optimal with respect to a particular cost function. However, for most systems the cost function is too complicated to give insight into the performance. Instead, let us restrict our view to what happens locally about equilibrium.

Near equilibrium, the Lie derivatives are approximated by

$$L_f V(x) \approx 2x^T PAx = x^T (PA + A^T P)x$$
$$L_g V(x) = 2x^T PB.$$

Thus, Sontag's feedback is given as

$$u = -\frac{x^T(PA + A^T P)x}{2x^T PB} - \frac{\sqrt{\left(x^T(PA + A^T P)x\right)^2 + (4x^T PBB^T Px)^2}}{2x^T PB}.$$

From the Riccati inequality

$$x^T PBB^T Px > x^T (PA + A^T P)x$$

and, therefore, if x is sufficiently small

$$4(x^T PBB^T Px) \gg x^T (PA + A^T P)x$$

and, hence, we can assume

$$\begin{aligned} u &\approx -\frac{x^T(PA + A^T P)x + 4x^T PBB^T Px}{2x^T PB} \\ &= -\frac{4x^T PBB^T Px}{2x^T PB} \\ &= -2B^T Px. \end{aligned} \tag{14}$$

Thus, locally about the origin, Sontag's feedback is approximately twice the LQR optimal feedback. While not a proof, the above argument suggests that the familiar process of tuning the LQR is applicable for tuning Sontag's feedback. The use of this LQ-CLF was first proposed by Fontaine [4] to construct the feedback

$$u = -g(x)^T Px. \tag{15}$$

Locally about the origin, it is trivial to show that this feedback is equivalent to the LQR. By including the nonlinear term $g(x)$ instead of its linearization, B, the authors of [4] are able to achieve better performance. For our system, the use of (15) offers no additional benefits over the LQR as $g(x) = B$; see (10). We, therefore, use Sontag's feedback instead as it incorporates the nonlinearities of both $f(x)$ and $g(x)$.

TABLE II
NUMERICAL VALUE OF THE MATRIX Q

Numerical value of Q	For
diag $[1e6, 4.7e4, 1e7]$	$z_{eq} = 1.0$ mm and $z_{eq} = 7.0$ mm
diag $[1e6, 6.6e4, 1e7]$	$z_{eq} = 2.0$ mm and $z_{eq} = 6.0$ mm
diag $[1e6, 1.2e5, 1e7]$	$z_{eq} = 3.0$ mm and $z_{eq} = 5.0$ mm
diag $[1e6, 5.3e5, 1e7]$	$z_{eq} = 4.0$ mm

The effect of tuning the matrix Q in (12) is seen in Fig. 4. The hovering point has been set to the mid-position and the matrix Q listed in Table II for $z_{\text{eq}} = 4$ mm is used. The (2, 2) element of Q is varied according to the value given in each subplot. Manipulating the penalty on velocity significantly increases the effective closed-loop damping. It should be noted that the oscillations are not caused by the controller, but rather the closed-loop response approaches the free response of the system as the (2, 2) element of Q is reduced.

Based on this procedure, we can select an appropriate LQ-CLF and compare the results with those obtained with (6), see Fig. 3. In Fig. 5, $z_{\text{eq}} = 2$ mm and the matrix Q is given in Table II. Using the LQ-CLF, we are able to dampen the response of the system and reduce the oscillations. Examining Fig. 5, the pertinent question is: why wasn't the controller able to eliminate or at least reduce the initial overshoot? The answer is that the controller is unable to eliminate the initial overshoot due to the physical limitations of the actuator. When released from rest against the upper coil, the armature swings to within 0.5 mm of the lower coil due to the potential energy stored in the springs. As the electromagnet is only capable of applying attractive forces, the controller is unable to affect the initial overshoot. In Section V-B, we explore how the releasing coil can be used to alleviate this problem.

Despite the initial overshoot, the LQ-CLF has several advantages that should not be overlooked. First, it is significantly easier to derive a CLF based on the algebraic Riccati equation than the one given in (6). While the matrix P_{nl} is derived from a Lyapunov equation, structuring the Lyapunov function in the form given in (6) requires insight into the dynamics of the system. In contrast, the LQ-CLF is formulated by simply linearizing the nonlinear system. Second, the LQ-CLF achieves better performance and the methodology for tuning is the same as the LQR, which is familiar to most control engineers. While it was somewhat possible to tune the performance with the original CLF, there is no clear methodology and it primarily involves trial and error.

B. Damping the Release

To remove the excess potential energy stored in the upper spring and thus dampen the armature motion, the upper coil must be utilized as the electromagnets are only capable of applying attractive forces. One solution would be to select a CLF that leads to a feedback that utilizes both magnetic coils. However, since the linearization of the system about any equilibrium below $z = 4$ mm does not depend on the upper coil, this is not possible using the method of Section V-A.

When hovering, the following methodology is used to dampen the release of the armature.

1) For both hovering above and below the mid-position, the voltage across the upper coil is set to -30 V until the armature has moved 0.1 mm away from the upper coil.
2) If the equilibrium position is at or above the mid-position, the closed-loop controller is activated after the armature has moved 0.1 mm away from the upper coil.
3) If the equilibrium position is below the mid-position, the voltage across the upper coil is set to 180 V until the armature is greater than 2 mm away from the upper coil. After this point, the voltage across the upper coil is set to zero and the closed-loop controller is activated. Once the estimated velocity reaches zero, the flux in the upper coil is driven to zero with the proportional controller

$$V_u = -5 \cdot 10^3 \lambda_u \tag{16}$$

since the armature has begun to move away from the lower coil and thus the upper coil can no longer affect the overshoot.

The goal of this procedure is to remove the excess potential energy stored in the upper spring. In 1), a release voltage of 30 V is used as it reduces the holding current quickly without making it difficult to dampen the release. If a larger voltage is used, it becomes difficult to bring the current back up as the electromagnets act as large inductors. If a smaller voltage is used, the release time becomes excessively long. The controller switches to the next step after the armature has moved 0.1 mm as this is the smallest change in position that can be reliably detected by the eddy current sensor. In the third item, voltage is only applied over the first 2 mm as the magnetic force generated by the upper coil rapidly decreases for large air gaps. The gain of the proportional controller given in (16) was selected experimentally to drive the flux to zero quickly without magnifying the effects of measurement noise.

The effectiveness of this releasing methodology is shown in Fig. 6. As with Fig. 5, $z_{\rm eq} = 2$ mm and the matrix Q is given in Table II.

VI. Linear Versus Nonlinear Control

Having shown in Section V-A that locally Sontag's feedback approximates the LQR, is there an advantage to using Sontag's feedback instead of the linear approximation given in (14)? To answer this question let us examine the nonlinear terms lost during linearization. The state space representation given in (2) can be expressed as

$$\frac{dx}{dt} = Ax + \Delta f(x) + Bu$$

where the matrices A and B are given by

$$A = \begin{bmatrix} 0 & 1 & 0 \\ -\frac{k_s}{m} & -\frac{b}{m} & -\frac{\lambda_{\rm eq}}{2k_a m} \\ -\frac{r\lambda_{\rm eq}}{2k_a} & 0 & -\frac{r(k_b+z_{\rm eq})}{2k_a} \end{bmatrix}$$

$$B = \begin{bmatrix} 0 & 0 & 1 \end{bmatrix}^T$$

and

$$\Delta f(x) = \begin{bmatrix} 0 & \frac{-x_3^2}{2k_a m} & -\frac{x_3 x_1 r}{k_a} \end{bmatrix}^T.$$

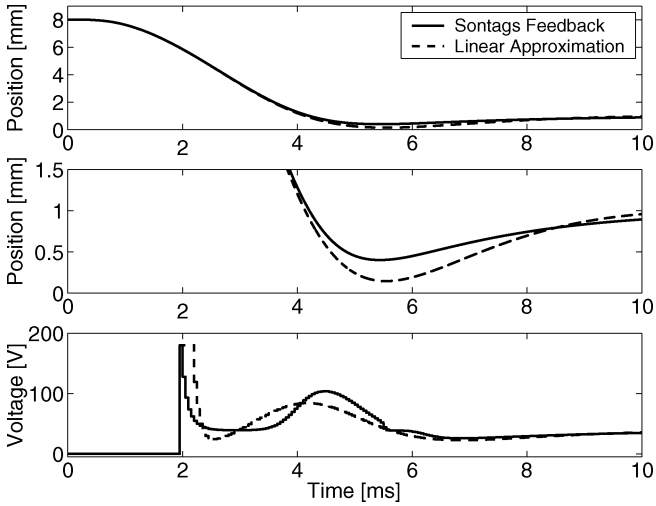

Fig. 7. Simulated response of the armature hovering 1 mm away from the magnetic coil.

The difference between the nonlinear and linear model, and thus to some extent Sontag's feedback and its linear approximation, are the terms contained in $\Delta f(x)$.

The loss of the third element of $\Delta f(x)$

$$-\frac{x_3 x_1 r}{k_a}$$

should not have a detrimental impact on the performance since it provides a stabilizing effect whenever $z > z_{\rm eq}$, which occurs for the majority of the armature travel. The loss of the second element of $\Delta f(x)$

$$\frac{-x_3^2}{2k_a m} \tag{17}$$

is not as benign since it provides a destabilizing effect. The loss of this term is most problematic whenever the value of x_3 is large. This typically occurs at the beginning of the transition when λ_l is initially zero since

$$x_3 = \lambda_l - \lambda_{\rm eq}.$$

Additionally, the effect is more prevalent for equilibrium positions near the electromagnet since $\lambda_{\rm eq}$ increases as $z_{\rm eq}$ decreases. Physically, the loss of the term given in (17) should result in more overshoot because the linear model (and thus the linear approximation of the feedback) underestimates the attractive force generated by the magnetic coil. Minimizing overshoot is an important consideration since excessive overshoot may lead to impacts between the armature and electromagnets.

Through simulation, the difference between Sontag's feedback and its linear approximation [see (14)] can be observed more easily in the absence of noise and other variations that occur on the experimental apparatus. Comparisons of the simulated response of Sontag's feedback and its linear approximation are given in Figs. 7–9 for several different equilibria. The controller used to dampen the release of the armature has been turned off to avoid obscuring the results.

As expected, the system experiences more overshoot in both Figs. 7 and 8 using the linear approximation of Sontag's feedback given in (14). In the case of hovering 0.5 mm away from the electromagnet, Fig. 8, this results in an impact between the

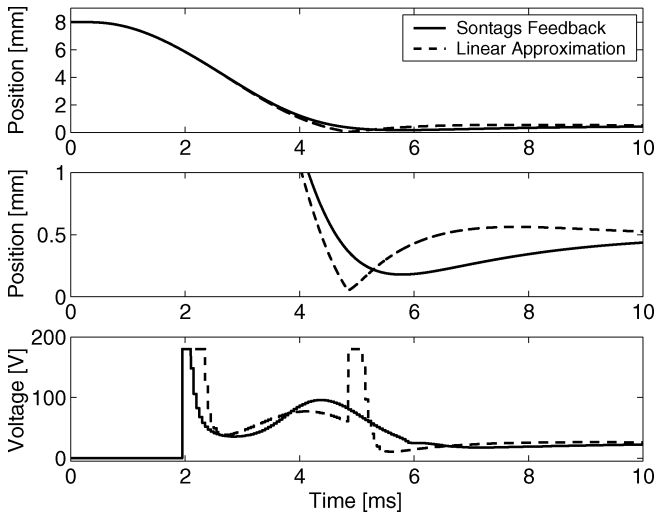

Fig. 8. Simulated response of the armature hovering 0.5 mm away from the magnetic coil.

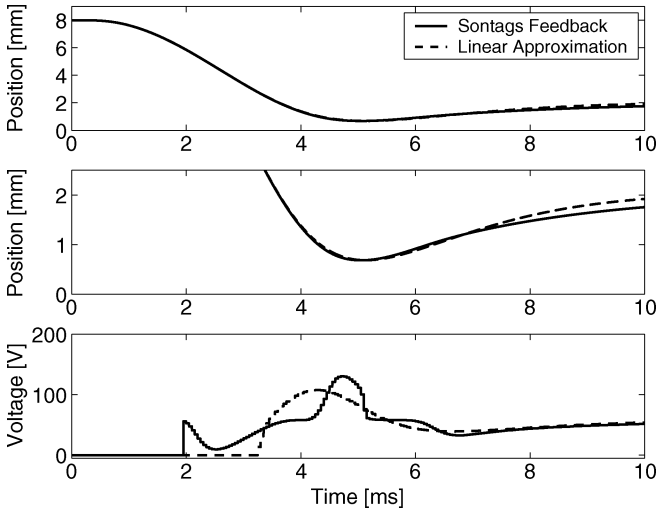

Fig. 9. Simulated response of the armature hovering 2 mm away from the magnetic coil.

armature and the magnetic coil at approximately 5 ms into the transition. The increased overshoot observed in Figs. 7 and 8 is caused by the application of larger voltages during the initial part of the transition. As mentioned before, this is expected as x_3 takes on its largest value at the beginning of the transition when $\lambda_l = 0$. Later in the transition, the voltage specified by the linear approximation tends to dip below Sontag's feedback in an attempt to compensate for the increased overshoot.

For equilibrium positions further away from the lower magnetic coil, the performance of Sontag's feedback and of its linear approximation appear to be more similar; see Fig. 9. Upon closer examination, the applied voltage determined by each controller is very different. To understanding why this difference arises, let us take a brief aside to discuss actuator saturation.

In addition to underestimating the attractive force generated by the magnetic coil, the loss of the term given in (17) may cause the controller to attempt to both "push" and "pull" on the

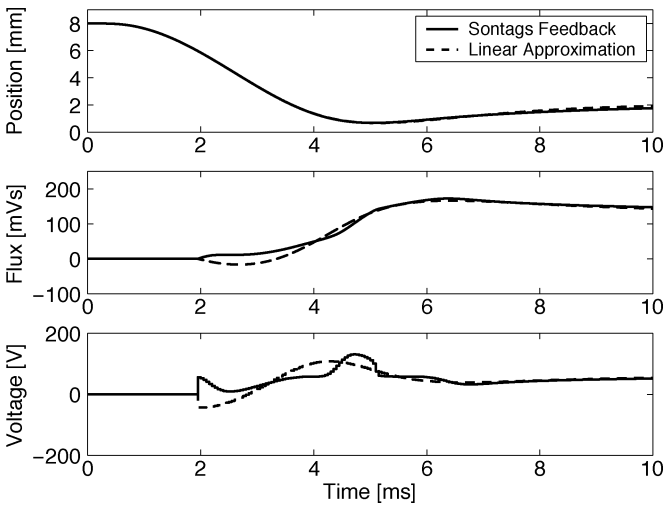

Fig. 10. Simulated response of the armature hovering 2 mm away from the magnetic coil without the saturation logic given in (19).

armature. The change in magnetic force for deviations about the equilibrium is given by

$$\Delta F_{\text{mag}} = \underbrace{\frac{-\lambda_{\text{eq}} x_3}{k_a}}_{\text{linear}} + \underbrace{\frac{-x_3^2}{2k_a}}_{\text{nonlinear}} . \tag{18}$$

During linearization, only the linear component of (18) remains. Therefore, ignoring the nonlinear dynamics, the electromagnet appears as if it can "push" on the armature by generating a sufficiently large negative value for x_3. This creates a potentially unstable feedback loop whereby the controller applies an attractive force in an attempt to repel the armature.

To avoid this, the following saturation logic is used:

$$V_l = \begin{cases} 180\text{ V}, & \text{if } V_l^{\text{fb}} > 180\text{ V} \\ V_l^{\text{fb}}, & \text{if } 0\text{ V} \le V_l^{\text{fb}} \le 180\text{ V} \\ V_l^{\text{fb}}, & \text{if } -180\text{ V} \le V_l^{\text{fb}} \le 0\text{ V and } \lambda_l \ge 5\text{ mVs} \\ -180\text{ V}, & \text{if } V_l^{\text{fb}} < -180\text{ V and } \lambda_l \ge 5\text{ mVs} \\ 0\text{ V}, & \text{if } V_l^{fb} \le 0\text{ V and } \lambda_l < 5\text{ mVs} \end{cases} \tag{19}$$

where V_l^{fb} is the voltage specified by the feedback. This allows the controller to apply negative voltages in order to reduce the flux if need be, but not to generate negative flux. Since the LQ-CLF is based on linearization, we expect that this problem may appear when using Sontag's feedback. However, since the nonlinearities are included in Sontag's feedback this problem should be less apparent than in the linear approximation.

Indeed, removing the saturation logic has less effect when using Sontag's feedback as shown in Fig. 10. The linear approximation of Sontag's feedback initially applies a negative voltage in an attempt to "push" on the armature. Despite the fact that this is avoided using the saturation logic given in (19), the use of Sontag's feedback remains advantageous as it applies a physically correct control signal earlier than does the linear controller, as shown in Fig. 9.

VII. Nonlinear Observer

As the actuator is intended for use in an automotive engine it is impractical to measure every state. The available measurements are the position of the armature and the current in each

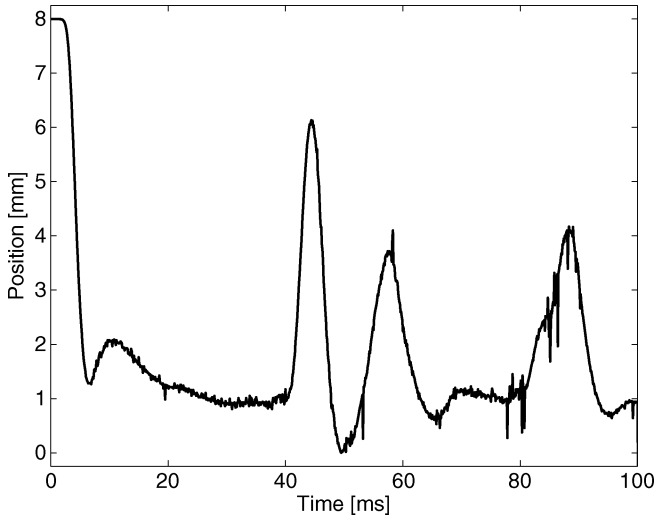

Fig. 11. Hovering achieved when magnetic saturation is neglected in the reconstruction of flux.

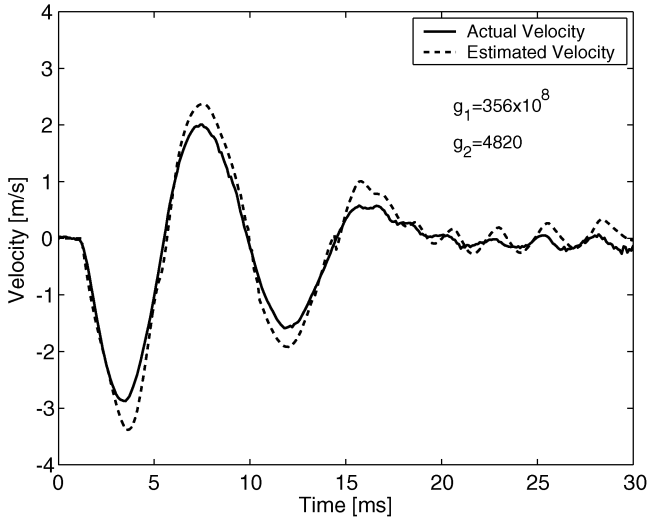

Fig. 12. Comparison of the actual versus estimated velocity.

coil. Current is chosen over flux as current sensors are standard in most power electronic devices and the compact design of the actuator prevents the mounting of hall effect sensors.

First, the magnetic flux is determined using a map of the magnetic force as a function of current and position developed by Wang [20], denoted as $F_{\mathrm{mag}}(i,z)$. Given the position and current, the magnetic flux is determined by

$$\lambda = \sqrt{2k_a F_{\mathrm{mag}}(i,z)} \tag{20}$$

based on (1). The advantage of using the mapping $F_{\mathrm{mag}}(i,z)$ is that saturation effects can be included by using look-up tables and/or piecewise continuous functions based on experimental data. If the experiment shown in Fig. 6 is repeated without including saturation effects in the mapping $F_{\mathrm{mag}}(i,z)$, the performance becomes significantly degraded as shown in Fig. 11.

Second, the armature velocity is estimated by the nonlinear observer

$$\begin{aligned}\frac{d\widehat{z}}{dt} &= \widehat{v} + \Gamma_1(z,\widehat{z})\\ \frac{d\widehat{v}}{dt} &= \frac{1}{m}\left(k_s(l-\widehat{z}) - b\widehat{v}\right) + \Gamma_2(i_l,i_u,z,\widehat{z})\end{aligned}$$

where

$$\begin{aligned}\Gamma_1(z,\widehat{z}) &= g_1(z-\widehat{z})\\ \Gamma_2(i_l,i_u,z,\widehat{z}) &= F^u_{\mathrm{mag}}(i_u,z) - F^l_{\mathrm{mag}}(i_l,z) + g_2(z-\widehat{z}).\end{aligned}$$

Computing the error dynamics, $e = \begin{bmatrix} z-\widehat{z} \\ v-\widehat{v}\end{bmatrix}$ results in

$$\frac{de}{dt} = \underbrace{\begin{bmatrix} 0 & 1 \\ -\frac{k_s}{m} & -\frac{b}{m}\end{bmatrix}}_{A_r} e + \begin{bmatrix} g_1 \\ g_2\end{bmatrix} \underbrace{\begin{bmatrix}1 & 0\end{bmatrix}}_{C_r} e$$

where the pair (A_r, C_r) is observable. Convergence of the estimated velocity is shown in Fig. 12. Numerically, the nonlinear observer is implemented on the dSpace board using an Euler approximation sampled at 20 kHz.

VIII. Experimental Results

The overall performance of the controller is presented in Fig. 13, which shows the armature hovering at several different

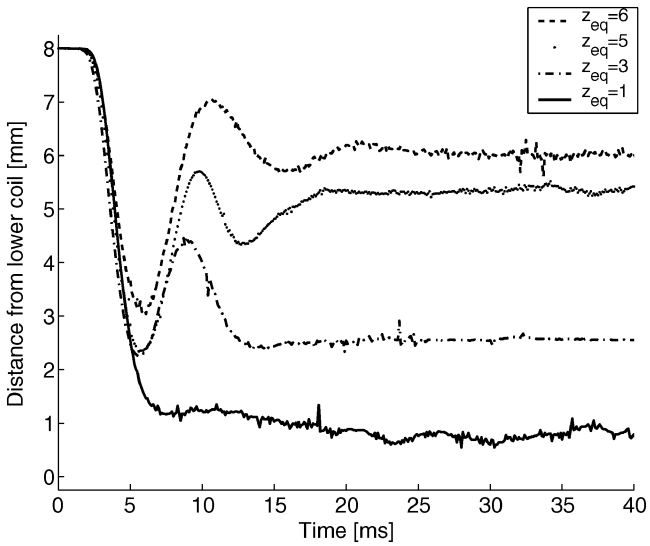

Fig. 13. Armature hovering at 1, 3, 5, and 6 mm away from the lower coil.

equilibrium positions. The controller is implemented using the measured position, the estimated velocity from the observer given in Section VII, the approximated flux using (20) based on the measured position and current, and the saturation logic given in (19). The Q matrices used in conjunction with (12) to select the CLFs for each equilibrium point are given in Table II. Recall that all equilibrium points less 1/3 the total lift (approximately 2.6 mm) away from either electromagnet are open-loop unstable [18]. As shown in Fig. 13, we are able to hover the armature approximately 1 mm away from the lower electromagnet.

The applied voltage and measured current response for the case of hovering 2 mm away from the electromagnet are shown in Fig. 14. These results are fairly representative of a typical response and illustrate three common features.

1) The controller typically saturates at the beginning of the transition as it attempts to quickly bring the current/flux up to its equilibrium value.

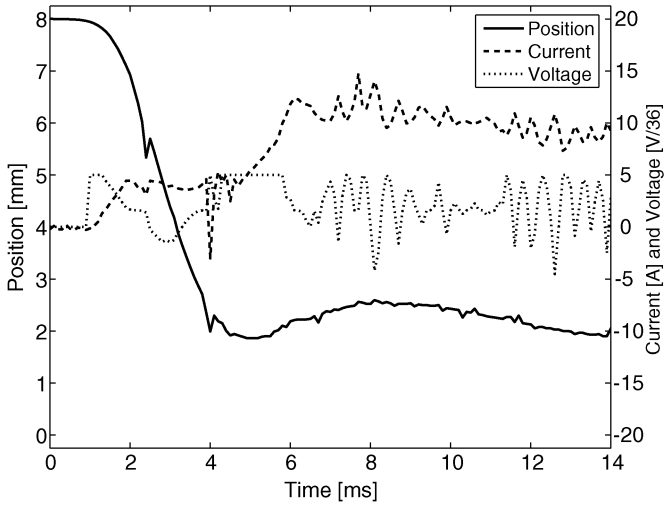

Fig. 14. Position, current, and voltage for the armature hovering 2 mm away from the lower coil, using the LQ-CLF controller.

2) The controller saturates again at approximately 4 ms as it attempts to prevent the armature from moving away from the lower coil.
3) At steady state, the noise from the current measurement can be seen in the applied voltage.

The first instance of saturation is caused by the initial large errors in the states x_1 and x_3. At the beginning of the transition, x_1 is large because the armature is far away from the magnetic coil and x_3 is large because the current/flux is initially zero. The voltage quickly reduces to a nonsaturated value once the current/flux is nonzero and the velocity begins to increase. The second instance of saturation occurs as the controller attempts to prevent the armature from moving away from the lower coil. This could be avoided by either increasing the penalty on position/flux or decreasing the penalty of velocity. By adjusting the penalties on the states in this manner, the controller tends to generate more flux as the armature approaches the lower coil. Thus deviations toward the mid-position could be decreased (and, thus, actuator saturation) at the expense of increased overshoot. To avoid potential impacts between the armature and magnetic coil, it was decided that minimizing overshoot was more important than avoiding actuator saturation. Finally, the current measurement is left unfiltered because the loss of bandwidth introduced by the filter was found to experimentally destabilize the controller.

IX. Conclusion

Stable hovering is achieved for a wide range of lift conditions for an EVA using Sontag's feedback. It was shown experimentally that by selecting the CLF based on the solution to an algebraic Riccati equation, it is possible to tune the performance of the controller using the familiar LQR procedure. By using Sontag's feedback instead of the LQR, we are able to include the nonlinear dynamics, resulting in improved performance with no additional work.

References

[1] A. Charara, J. DeMiras, and B. Caron, "Nonlinear control of a magnetic levitation system without premagnetization," *IEEE Trans. Contr. Syst. Technol.*, vol. 4, no. 5, pp. 513–523, Sep. 1996.
[2] D. Cho, Y. Kato, and D. Spilman, "Sliding mode and classical control of magnetic levitation systems," *IEEE Contr. Syst. Mag.*, vol. 13, no. 1, pp. 42–48, Feb. 1993.
[3] B. Fabien, "Observer-based feedback linearization control of an electromagnetic suspension," *ASME J. Dyn. Syst., Meas. Contr.*, vol. 118, pp. 615–619, Sep. 1996.
[4] D. Fontaine, S. Liao, J. Paduano, and P. Kokotovic, "Nonlinear control experiments on an axial flow compressor," in *Proc. IEEE Conf. Decision Contr.*, vol. 2, Dec. 2000, pp. 1329–1334.
[5] L. Gentili and L. Marconi, "Robust nonlinear disturbance suppression of a magnetic levitation system," *Automatica*, vol. 39, no. 4, pp. 735–742, April 2003.
[6] S. Green and K. Craig, "Robust, digital nonlinear control of magneticlevitation systems," *ASME J. Dyn. Syst., Meas. Contr.*, vol. 120, no. 4, pp. 488–495, Dec. 1998.
[7] H. Khalil, *Nonlinear Systems*, 2nd ed. Englewood Cliffs, NJ: Prentice Hall, 1996.
[8] M. Levin and M. Schechter, "Camless Engine,", 1996.
[9] J. Lindlau and C. Knospe, "Feedback lineariztion of active magnetic bearing with voltage control," *IEEE Trans. Contr. Syst. Technol.*, vol. 10, no. 1, pp. 21–31, Jan. 2002.
[10] L. Mao and J. Li, "Feedback linearization of magnetic bearing actuators for a uniform upper bound of force slew rate," in *Proc. IEE Electr. Power Applicat.*, vol. 146, Jul. 1999, pp. 378–382.
[11] C. Munaro, M. Filho, R. Borges, S. Munareto, and W. DaCosta, "Modeling and observer-based nonlinear control of a magnetic levitation system," in *Proc. IEEE Conf. Contr. Applicat.*, vol. 1, Sep. 2002, pp. 162–167.
[12] K. Peterson and A. Stefanopoulou, "Rendering the electromechanical valve actuator globally asymptotically stable," in *Proc. IEEE Conf. Decision Contr.*, vol. 2, Dec. 2003, pp. 1753–1758.
[13] A. Rundell, S. Drakunov, and R. DeCarlo, "A sliding mode observer and controller for stabilization of rotational motion of a vertical shaft magnetic bearing," *IEEE Trans. Contr. Syst. Technol.*, vol. 4, no. 5, pp. 598–608, Sep. 1996.
[14] R. Sepulchre, M. Jankovic, and P. Kokotovic, *Constructive Nonlinear Control*. New York: Springer-Verlag, 1997.
[15] K. Shibukawa, T. Tsubakiji, and H. Kimura, "Robust stabilization of a magnetic levitation system," in *Proc. IEEE Conf. Decision Contr.*, vol. 3, Dec. 1991, pp. 2368–2371.
[16] R. Smith and W. Weldon, "Nonlinear control of a rigid rotor magnetic bearing system: modeling and simulation with full state feedback," *IEEE Trans. Magn.*, vol. 31, no. 2, pp. 973–980, Mar. 1995.
[17] E. Sontag, "A universal construction of artstein's theorem on nonlinear stabilization," *Syst. Contr. Lett.*, vol. 13, no. 2, pp. 117–123, Aug. 1989.
[18] C. Tai and T. Tsao, "Control of an electromechanical camless valve actuator," in *Proc. Amer. Contr. Conf.*, vol. 1, May 2002, pp. 262–267.
[19] M. Velasco-Villa, R. Castro-Linares, and L. Corona-Ramirez, "Modeling and passivity based control of a magnetic levitation system," in *Proc. IEEE Conf. Contr. Applicat.*, Sep. 2001, pp. 64–69.
[20] Y. Wang, A. Stefanopoulou, M. Haghgooie, I. Kolmanovsky, and M. Hammoud, "Modeling of an electromechanical valve actuator for a camless engine," in *Proc. Int. Symp. Adv. Vehicle Contr.*, Aug. 2000.
[21] J. Yi, K. Park, S. Kim, Y. Kwak, M. Abdelfatah, and I. Busch-Vishniac, "Force control of magnetic levitation system using flux density measurement," in *Proc. IEEE Conf. Decision Contr.*, vol. 3, Dec. 1995, pp. 2153–2158.